Photosynthesis Models

A Biomimetic Model of the Electron Transfer between P_{680} and the TyrZ–His190 Pair of PSII**

Fabien Lachaud, Annamaria Quaranta, Yann Pellegrin, Pierre Dorlet, Marie-France Charlot, Sun Un, Winfried Leibl,* and Ally Aukauloo**

In memory of G. T. Babcock

The tyrosyl/tyrosine redox couple has been well established as a crucial cofactor for several enzymatic systems.[1] In the case

[*] F. Lachaud, Y. Pellegrin, Dr. P. Dorlet, Dr. M.-F. Charlot, Prof. Dr. A. Aukauloo
Laboratoire de Chimie Inorganique
Bât. 420, Université Paris-Sud
91405 Orsay (France)
Fax: (+33) 1-6915-4754
E-mail: pierdorlet@icmo.u-psud.fr
aukauloo@icmo.u-psud.fr

Dr. A. Quaranta, Dr. S. Un, Dr. W. Leibl
Service de Bioénergétique, CEA Saclay
Bât. 532, 91191 Gif-sur-Yvette CEDEX (France)
Fax: (+33) 1-6908-8717
E-mail: leibl@dsvidf.cea.fr

Dr. A. Quaranta
Muséum National d'Histoire Naturelle
Laboratoire de Chimie et de Biochimie des Substances Naturelles
UMR 5154 CNRS/USM 0502 CNRS
63 rue Buffon, 75005 Paris (France)

[**] This work was supported by the CNRS (Programme Energie, PRI4), the CEA for the LRC project (LRC-CEA no. 33V), and the European Commission (STRP SOLAR-H 516510). A.Q. acknowledges the European Commission for financial support (contract "Wonderfull" HPRN-CT-2002-00177). We thank the Centre Informatique National de l'Enseignement Supérieur, Montpellier, France for computation time.

Supporting information for this article is available on the WWW under http://www.angewandte.org or from the author.

  DOI: 10.1002/ange.200461948

of the photosynthetic reaction center of photosystem II (PSII) it has been argued that a histidine residue (His190) in close proximity to tyrosine Z (TyrZ) is essential to drive electron transfer from TyrZ to the P_{680}^{+} primary donor ion; otherwise, the reaction would be energetically unfavorable. The decreased ionization potential of this pair is explained by hydrogen bonding and the proton coupled electron transfer process (PCET).[2] The recently acquired X-ray crystallographic structure of PSII from the cyanobacterium *Thermosynechococcus elongatus*, shows that the TyrZ and His190 residues in the catalytic state are not coordinated to the metal ions. They are probably not involved in the proton exit from the oxygen evolving complex (OEC), as no hydrogen-bonding chain has been detected that would allow the proton from TyrZ to leave the active site.[3] In light of the crystallographic data, it appears that the "rocking proton" mechanism between these two amino acids is favored in the electron transfer steps of the PSII catalytic cycle.

A synthetic model of PSII has recently been proposed, in which a $[Ru(bpy)_3]^{2+}$ chromophore plays the role of P_{680}.[4] Photoinduced electron transfer from a covalently attached modified tyrosine residue to the bipyridine group has been shown, but direct evidence for the influence that both the hydrogen bond and the Ru^{II} metal ion have on the electrochemical properties of the modified tyrosine has not yet been established. Herein we report a new molecular system that serves as a closer biomimetic model for the TyrZ–His190 pair (a hydrogen-bonded phenol–imidazole interaction). The model is attached to a chelating phenanthroline group, which serves as an anchoring site for the photoactive Ru^{II} chromophore (compound **1**). Compounds **2**–**4** have been studied to account for the physical behavior of the parent compound **1**. The corresponding Ru-**1**–Ru-**3** complexes were prepared, and their electrochemical and photophysical properties were studied. The family of ligands was synthesized by

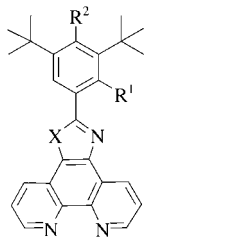

1: R^1 = OH, R^2 = H, X = NH
2: R^1 =H, R^2 = OH, X = NH
3: R^1 = R^2 = H, X = NH
4: R^1 = OH, R^2 = H, X = O

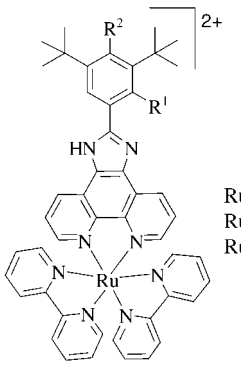

Ru-**1**
Ru-**2**
Ru-**3**

following the procedure of Steck and Day (Supporting Information).[5] Compound **4** was obtained as a by-product in the synthesis of **1**.

Regardless of solvent polarity, the electronic spectrum of **1** shows a distinct structured absorption band between 300 and 380 nm, indicative of a rigid molecular framework. This supports the fact that the two aromatic rings adopt a coplanar orientation in solution through a strong intramolecular hydrogen bond between the phenolic OH group and the imidazole nitrogen atom.[6] This is confirmed by the ^{1}H NMR spectrum of **1** in [D$_6$]DMSO, in which a dissymmetry of the phenanthroline protons is apparent. In the solid state, the presence of intramolecular hydrogen bonding is supported by the absence of OH group vibration characteristics in the IR spectrum of **1**; indeed these features are present in the IR spectroscopy data for **2** (Supporting Information).

Cyclic voltammograms (CV) of **1** and **4** in CH_2Cl_2 show a first oxidation process (E_{pa}) at 0.90 and 1.10 V versus standard calomel electrode (SCE) respectively, which corresponds to the process of phenoxyl radical formation from phenol. These values are lower than those observed for hydrogen-bond-free phenol,[7] and are consistent with previous examples in which the phenolic OH group is hydrogen bonded to a nearby base.[8] The difference in the E_{pa} values for **1** and **4** can be explained by the higher basicity of the imidazole group relative to oxazole. Under the experimental conditions reported herein, the first electron-transfer process was found to be quasireversible in nature. Cathodic shifts in the oxidation potentials were observed in CV experiments performed under basic conditions (1 equivalent NBu_4OH), which indicates the greater ease with which phenolate groups oxidize. Interestingly, a lower potential was observed for $\mathbf{4}^{1-}$ (+0.18 V) than for $\mathbf{1}^{1-}$ (+0.30 V), which can be rationalized by the presence of a hydrogen bond between the imidazole proton and the deprotonated phenol in $\mathbf{1}^{1-}$. Moreover, the higher values for the oxidation of $\mathbf{1}^{1-}$, $\mathbf{2}^{1-}$ (0.00 V), and $\mathbf{4}^{1-}$ relative to the reference compound 2,4,6-tri-(*tert*-butyl)phenolate imply a decreased electron density on the phenol ring, and thus partial delocalization on the imidazole or oxazole groups.

Ruthenium complexes Ru-**1**, Ru-**2** and Ru-**3** were synthesized and characterized by standard spectroscopic techniques (Supporting Information). The electrochemical data are given in Table 1. On the cathodic side of the CV during the scan down to −1.9 V versus SCE, only two redox waves were observed instead of the three one-electron reduction processes that are typical for $[Ru(bpy)_3]^{2+}$ under the same conditions. This indicates that the modified phenanthroline end is less-readily reduced owing to the electron-rich imidazole ring. No electronic influence was observed on the $Ru^{III/II}$ couple at 1.26 V, a typical value for a ruthenium(II) trisbipyridine complex. However, the most interesting feature of the CV is the first reversible oxidation wave (+0.52 V versus SCE) which corresponds to the oxidation of the phenol group. The shift toward a less-positive potential for the same

Table 1: Half-wave potentials for the oxidation (^{ni}E) and reduction (^{n}E) of Ru-**1**, Ru-**2**, and Ru-**3**.[a]

Compound	^{II}E	^{I}E	^{i}E	^{ii}E[b]	^{iii}E
Ru-**1**	−1.60	−1.40	0.58	1.08	1.29
Ru-**2**	−1.63	−1.41	0.38[b]	1.09	1.40
Ru-**3**	−1.63	−1.41		1.10	1.40

[a] Determined by CV at 100 mV s^{-1} in CH_2Cl_2; $E = 1/2(E_{pa} + E_{pc})$ in V versus SCE in the presence of $TBAClO_4$. TBA = tetra-*n*-butylammonium. [b] Nonreversible.

process relative to the free ligand can be interpreted as a weakening of the O–H bond through an inductive effect of the Ru^{II} ion. Furthermore, the reversible nature of this wave may imply that the coordinated phenanthroline cavity cannot play the role of a proton trap, as is the case of the free ligand. Hence, as mentioned before, this is a clear example in which the presence of a divalent cation (Ru^{II}; not directly coordinated to a phenol moiety), together with a hydrogen-bonded phenol group, lowers the oxidation potential of the phenoxyl/phenol couple by more than 300 mV. The second wave at 1.1 V was assigned to the oxidation of the imidazole ring, and was confirmed by the CV of Ru-**3**. The electrochemical behavior of Ru-**1** is supported by density functional theory (DFT) calculations, which were carried out with the hybrid functional B3LYP[9] as implemented in the Gaussian98 program[10] and a LanL2DZ[11] effective potential basis for all atoms. The geometry of the complex was optimized starting from the totally optimized geometry of the constitutive ligands. Indeed, the calculated HOMO for Ru-**1** is localized primarily on the phenol ring.

The singly oxidized species of Ru-**1** and Ru-**2** (Ru-**1**$^{\bullet}$ and Ru-**2**$^{\bullet}$, respectively) were prepared electrochemically and characterized by high-field/high-frequency EPR spectroscopy. Figure 1 shows the spectra obtained at 285 GHz for

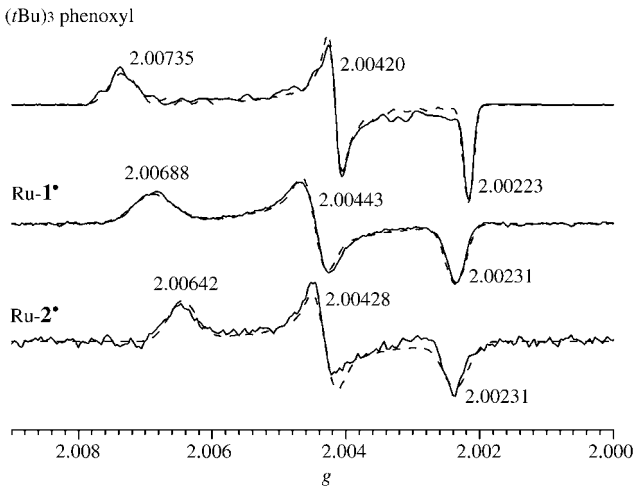

Figure 1. Experimental (solid line) and simulated (dashed line) EPR spectra (285 GHz) of the 2,4,6-tri-(*tert*-butyl)phenoxyl, Ru-**1**$^{\bullet}$, and Ru-**2**$^{\bullet}$ radicals. Ru-**1**$^{\bullet}$ and Ru-**2**$^{\bullet}$ were prepared electrochemically in dichloromethane. The 2,4,6-tri-(*tert*-butyl)phenoxyl radical was prepared by chemical oxidation of 2,4,6-tri-(*tert*-butyl)phenol in CH_3CN solution with aqueous potassium ferricyanide and sodium hydroxide. Experimental conditions: $\nu_{mw} = 285.090$ GHz, $T = 4.2$ K, modulation amplitude 0.95 mT.

the solutions of Ru-**1**$^{\bullet}$ and Ru-**2**$^{\bullet}$ together with the simulated spectra. As a reference, the 285-GHz spectrum of the chemically oxidized 2,4,6-tri-(*tert*-butyl)phenoxyl radical is shown, which can be considered as a generic model for non-hydrogen-bonded 2,4,6-trisubstituted-phenoxyl radicals. The *g* anisotropy for these radicals is clearly resolved at 285 GHz, and the *g* values obtained from fitting the data are indicated. The *g* values for Ru-**1**$^{\bullet}$ and Ru-**2**$^{\bullet}$ are indeed close to those of the 2,4,6-tri-(*tert*-butyl)phenoxyl radical, and confirm that the phenol portion of the ligand is, in fact, the locus of oxidation. The smaller g_x value observed for Ru-**2**$^{\bullet}$ relative to Ru-**1**$^{\bullet}$ can be attributed to the more delocalized spin density in the case of Ru-**2**$^{\bullet}$. A more detailed HFEPR study regarding the influence of the hydrogen bond and the inductive effect of the Ru^{II} ion on the *g* values of the phenoxyl radical in this type of complex is currently underway.

The electronic absorption spectrum of Ru-**1** is shown in Figure 2. The spectrum shows features both of the ligand and

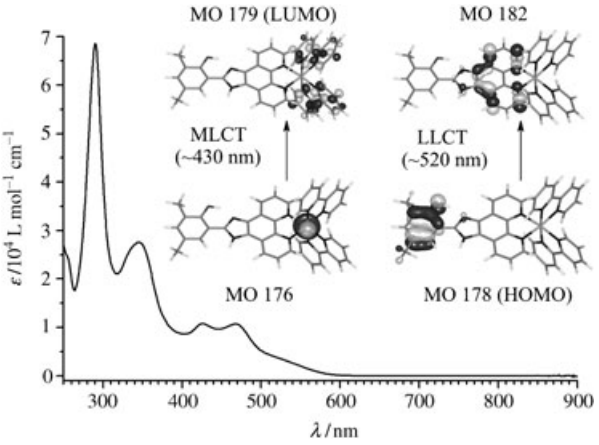

Figure 2. Electronic spectrum of Ru-**1** in CH_2Cl_2 and the calculated frontier molecular orbitals involved in the calculated MLCT and LLCT transitions (see text).

the ruthenium chromophore. Preliminary results from time-dependent DFT (TD DFT) calculations[12] confirmed that the MLCT band from the t_{2g} orbitals of Ru^{II} to the bpy*-based MOs falls within the 450-nm wavelength range observed for $[Ru(bpy)_3]^{2+}$. Through our calculations, we attribute the shoulder observed to the MLCT band that tails up to 570 nm to a ligand–ligand charge transfer from the phenol extremity (MO178: HOMO) to the coordinating phenanthroline (MO182: LUMO + 3). The MOs involved for these transitions are shown in Figure 2.

Upon excitation in the MLCT band, Ru-**1**, Ru-**2**, and Ru-**3** show an emission band that peaks at ≈ 600 nm, with quantum yields and lifetimes (≈ 1 μs) similar to those for $[Ru(bpy)_3]^{2+}$. In the region investigated, the transient absorption spectra of the three complexes also exhibit the typical depletion band at 450 nm, which corresponds to the absorption maximum of the MLCT band of $[Ru(bpy)_3]^{2+}$. This suggests that the excited state of these complexes is similar to that of $[Ru(bpy)_3]^{2+}$, despite the differences in the coordinated ligand. There is no evidence of intramolecular reactions that occur between the chromophore and the ligand, as expected from the electron-donating character of the phenol–imidazole groups.

To investigate whether the oxidized state of the chromophore is able to oxidize the ligand, electron-transfer experiments in the presence of MV^{2+} as an external electron acceptor were performed (MV = methyl viologen). The transient absorption spectra of Ru-**1**, Ru-**2,** and Ru-**3** are dominated by the strong absorption of $MV^{\bullet+}$, with peaks at 390 nm and 600 nm. However, $MV^{\bullet+}$ has an absorption

minimum at 450 nm, where the recovery of the ground-state absorption of the chromophore could be monitored. The positive absorption changes that occur in the traces at 450 nm for Ru-**1** and Ru-**2** are reminiscent of the formation of a phenoxyl radical. The kinetics for all complexes show a recovery of the reduced state of the chromophore within 0.5 μs (Figure 3). This is much faster than the decay of $MV^{\bullet+}$,

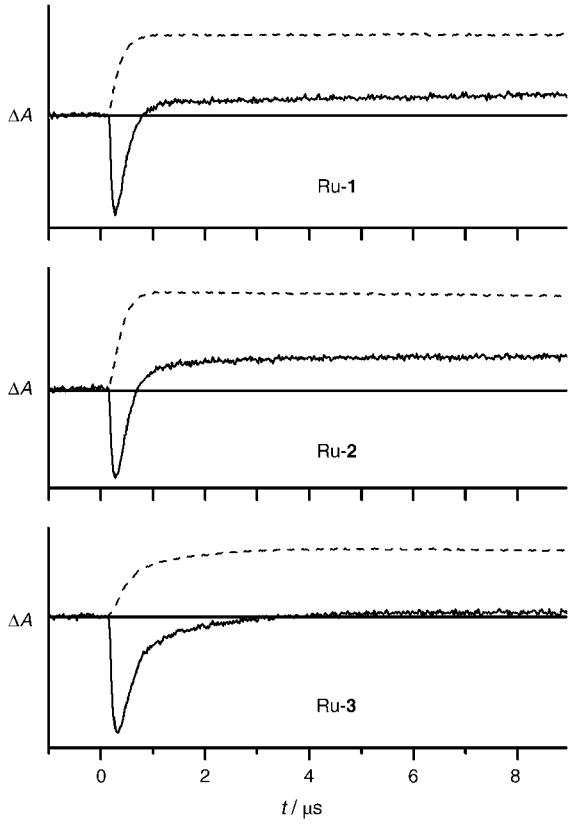

Figure 3. Time-resolved absorption changes at 600 nm (dashed lines) and 450 nm (solid lines) of complexes Ru-**1**, Ru-**2**, and Ru-**3** upon excitation with nanosecond laser flashes at 355 nm in aqueous, Ar-saturated solution (HEPES, 10 mM, pH 7). MV^{2+} (10 mM) was present as an external electron acceptor.

which occurs in about 200 μs, as monitored at 600 nm. This indicates that the reduction of Ru^{III} to Ru^{II} is the result of an electron transfer from an electron-donating group on the ligand. The apparent kinetics of the recovery phase of the absorption at 450 nm is similar to the rate of electron transfer from the chromophore to MV^{2+}, which indicates that formation of the Ru^{III} oxidation state is rate limiting and that the intrinsic rate of intramolecular electron transfer is faster.

An ethanolic solution of Ru-**1** was irradiated with white light in the presence of excess $[Co(NH_3)_5Cl]^{2+}$, an irreversible electron acceptor in water. The EPR spectrum (9 GHz) of the frozen sample exhibits a single line centered at $g_{iso} = 2.004$ (Figure 4), with no resolved hyperfine structure and a peak-to-trough width of 0.9 mT. This is in good agreement with EPR spectra obtained for hydrogen-bonded phenoxyl radical[8] and the 9-GHz spectrum of the electrolyzed sample of

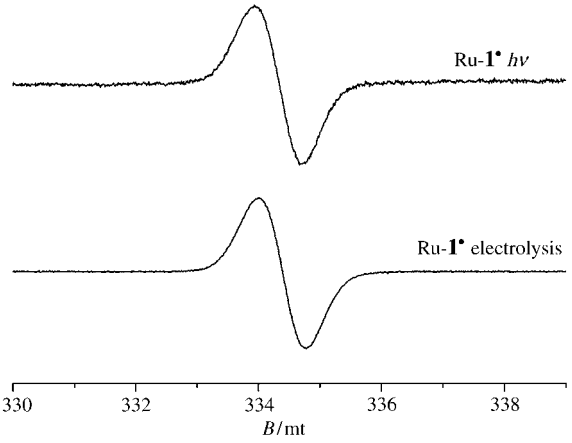

Figure 4. EPR spectra (9 GHz) of the photogenerated (top) and electrochemically prepared (bottom) Ru-**1**• radicals. Experimental conditions: $\nu_{mw} = 9.38009$ GHz (top), $\nu_{mw} = 9.38225$ GHz (bottom), $P_{mw} = 16$ μw, modulation amplitude 0.4 mT, modulation frequency 100 kHz, $T = 100$ K.

Ru-**1**• characterized by HFEPR (Figure 1). The low concentration of the photogenerated radical did not permit the observation of the EPR signal at 285 GHz. However, the isotropic *g* value determined with the 9-GHz spectrum and the comparison with the spectrum of Ru-**1**• obtained by preparative electrolysis are fully consistent with a phenoxyl radical.

The EPR signature of the radical formed under photoaccumulation in conjunction with the positive absorption changes at 450 nm for times over 1 μs clearly show a photoinduced electron transfer from a hydrogen-bonded phenol–imidazole pair to generate a phenoxyl radical. Further work with systems in which this phenol–imidazole pair is used as an electron relay between Ru^{II} and a manganese complex is underway.

Experimental Section

Typical procedure: $Ru(bpy)_2Cl_2$ (100 mg, 0.2 mmol) was treated with $AgNO_3$ (65.6 mg, 0.4 mmol) in MeOH (5 mL) for 1 h. The AgCl precipitate was filtered off, and the filtrate evaporated to dryness. Ligand **1** (85 mg, 0.2 mmol) was added to the ruthenium salt in MeOH (10 mL) and stirred at reflux for 3 h. The solvent was removed by rotary evaporation and the crude product was purified by column chromatography on neutral alumina (CH_2Cl_2/MeOH 90:10) to afford Ru-**1** (102 mg, 61%) as an orange solid. IR (KBr): $\tilde{\nu} = 2950$ (C–H), 1713 (C=N), 1360 cm^{-1} (N=O, NO_3^-); UV/Vis (CH_2Cl_2): λ_{max} (ε) = 290 (68500), 345 (27800), 430 (10750), 465 (10650), 520 nm (3800); ^{1}H NMR (250 MHz, [D$_6$]DMSO): $\delta = 8.99$ (d, 2H), 8.85 (t, 4H), 8.29 (d, 1H), 8.19 (t, 2H), 8.08 (t, 2H), 7.84 (d, 2H), 7.80 (d, 2H), 7.75(d, 1H), 7.70 (d, 1H), 7.57 (dd, 4H), 7.36 (t, 2H), 7.18 (d, 1H), 1.46 (s, 9H), 1.34 ppm (s, 9H); ESI MS: *m*/*z* (%): 419.0 (100) $[M]^{2+}$; elemental analysis: calcd for $C_{47}H_{44}N_{10}O_7Ru$: C 58.7, H 4.6, N 14.6; found: C 59.3, H 4.7, N 14.9.

Received: September 10, 2004
Published online: January 28, 2005

Keywords: artificial photosynthesis · biomimetic synthesis · phenoxyl radicals · photochemistry · ruthenium

[1] J. A. Stubbe, W. A. van der Donk, *Chem. Rev.* **1998**, *98*, 705 – 762.
[2] a) K. L. Westphal, C. Tommos, R. I. Cukier, G. T. Babcock, *Curr. Opin. Plant Biol.* **2000**, *3*, 236 – 242; b) C. W. Hoganson, G. T. Babcock, *Science* **1997**, *277*, 1953 – 1956.
[3] K. N. Ferreira, T. M. Iverson, K. Maghlaoui, J. Barber, S. Iwata, *Science* **2004**, *303*, 1831 – 1838.
[4] a) M. Sjödin, S. Styring, B. Akermark, L. Sun, L. Hammarström, *J. Am. Chem. Soc.* **2000**, *122*, 3932 – 3936; b) D. Burdinski, K. Wieghardt, S. Steenken, *J. Am. Chem. Soc.* **1999**, *121*, 10781 – 10787.
[5] E. A. Steck, A. R. Day, *J. Am. Chem. Soc.* **1943**, *65*, 452 – 456.
[6] M. Mosquera, J. C. Penedo, M. C. Rios Rodriguez, F. Rodriguez-Prieto, *J. Phys. Chem.* **1996**, *100*, 5398 – 5407.
[7] F. G. Bordwell, J. P. Cheng, *J. Am. Chem. Soc.* **1991**, *113*, 1736 – 1743.
[8] a) L. Benisvy, A. J. Blake, D. Collison, E. S. Davies, C. D. Garner, E. J. L. McInnes, J. McMaster, G. Whittaker, C. Wilson, *Dalton Trans.* **2003**, 1975 – 1985; b) T. Maki, Y. Araki, Y. Ishida, O. Onomura, Y. Matsumura, *J. Am. Chem. Soc.* **2001**, *123*, 3371 – 3372.
[9] a) A. D. Becke, *J. Chem. Phys.* **1993**, *98*, 5648 – 5652; b) C. T. Lee, W. T. Yang, R. G. Parr, *Phys. Rev. B* **1988**, *37*, 785 – 789.
[10] Gaussian 98 (Revision A.7), M. J. Frisch, G. W. Trucks, H. B. Schlegel, G. E. Scuseria, M. A. Robb, J. R. Cheeseman, V. G. Zakrzewski, J. A. Montgomery, R. E. Stratmann, J. C. Burant, S. Dapprich, J. M. Millam, A. D. Daniels, K. N. Kudin, M. C. Strain, O. Farkas, J. Tomasi, V. Barone, M. Cossi, R. Cammi, B. Mennucci, C. Pomelli, C. Adamo, S. Clifford, J. Ochterski, G. A. Petersson, P. Y. Ayala, Q. Cui, K. Morokuma, D. K. Malick, A. D. Rabuck, K. Raghavachari, J. B. Foresman, J. Cioslowski, J. V. Ortiz, B. B. Stefanov, G. Liu, A. Liashenko, P. Piskorz, I. Komaromi, R. Gomperts, R. L. Martin, D. J. Fox, T. Keith, M. A. Al-Laham, C. Y. Peng, A. Nanayakkara, C. Gonzalez, M. Challacombe, P. M. W. Gill, B. G. Johnson, W. Chen, M. W. Wong, J. L. Andres, M. Head-Gordon, E. S. Replogle, J. A. Pople, Gaussian, Inc., Pittsburgh, PA, **1998**..
[11] a) T. H. Dunning, Jr, P. J. Hay, *Modern Theoretical Chemistry*, *Vol. 3*, Plenum, New York, **1976**; b) P. J. Hay, W. R. Wadt, *J. Chem. Phys.* **1985**, *82*, 270 – 283; c) P. J. Hay, W. R. Wadt, *J. Chem. Phys.* **1985**, *82*, 299 – 310; d) W. R. Wadt, P. J. Hay, *J. Chem. Phys.* **1985**, *82*, 284 – 298.
[12] a) M. E. Casida, C. Jamorski, K. C. Casida, D. R. Salahub, *J. Chem. Phys.* **1998**, *108*, 4439 – 4449; b) S. R. Stoyanov, J. M. Villegas, D. P. Rillema, *Inorg. Chem. Commun.* **2004**, *7*, 838 – 841; c) H. Zabri, I. Gillaizeau, C. A. Bignozzi, S. Caramori, M. F. Charlot, J. Cano-Boquera, F. Odobel, *Inorg. Chem.* **2003**, *42*, 6655 – 6666.

